Patterns of Reservoir Triggered Seismicity in a Slow Tectonic Context (France)

J-R Grasso[1], A. Karimov[1], D. Amorese[2,3], C. Sue[4], C. Voisin[1]

[1] ISterre, Université de Grenoble-Alpes, France
[2] Observatoire Volcanologique et Sismologique de Guadeloupe, Institut de Physique du Globe de Paris, UMR 7154 CNRS, Le Houëlmont, 97113 Gourbeyre, La Guadeloupe, France
[3] Dpt Biologie et Sciences de la Terre, Université de Caen-Normandie, 14 032 Caen Cedex, France
[4] UMR6249-UBFC Université de Franche-Comté, France

Abstract
In a context of a slow tectonic activity of continental France, we analyze the impact of the 26 largest impounded reservoirs on the seismicity patterns. Similarly to tectonic earthquake interactions, we select 1-3 reservoir lengths as a proxy for the distance where the stress change induced by reservoir impoundments may trigger seismicity. We use the reservoir length, (L_r), as the equivalent of a mainshock fault length, this later controlling the triggering zone for tectonic aftershock location. Accordingly we define $1L_r$-distance as the near field reservoir effect on seismicity, and the $10L_r$-distance as the far field, null, effect of reservoir stress change on background seismicity.
We find that (i) about a quarter of the reservoirs, (6 reservoir dams), trigger M_{max}=2.5-4.7 seismic sequence within 1Lr - 15 years space-time window; (ii) as tested against randomized series, superposed epoch analysis resolves a robust increase in average seismicity rate within 2 years – $1\text{-}3L_r$ distance from reservoirs.
The reservoirs that trigger in the ($1L_r$) near field are significantly larger as estimated by length values than the non-triggering ones. The normalized distance is a more efficient parameter to identify $1L_r$ trigger reservoirs than the absolute distance-to-reservoirs, respectively. From a reservoir dimension approach the reservoir length supports the size of the area where the stresses change is more important to control the earthquake triggering than the value of the stress change (estimated using the reservoir depth). Our results suggest the RTS mimics the aftershock sequence of a slow reservoir impoundment loading, with a corresponding $M^*_{reservoir}=M(L_r)$ mainshock magnitude. Similarly to mainshock-aftershock interactions, our analysis and observations support the M_{max} value for RTS on a given reservoir remains, in average, smaller than the reservoir magnitude equivalent.

Introduction:

Understanding and managing induced and triggered seismicity is a key challenge for many geo-resource applications. Most of the current concerns related to seismic instabilities induced by geo-resource production are due to fluid manipulation. The drastic rise in seismicity in North America (e.g. Oklahoma, Western Canada) is an unintended consequence of human-made fluid handling (e.g. Ellsworth et al. 2013; Atkinson et al., 2016). The earthquake swarms related to disposal of wastewater by injection below the productive reservoir (e.g. Central US, Ellsworth et al. 2013; van der Elst et al. 2013)) are not yet understood in term of

space and time and size distributions. The time and space evolutions of earthquake swarms related to disposal of waste water by injection below the productive reservoir (e.g. Central US, Ellsworth et al. 2013) are difficult to deterministically relate to specific well history, due to the current inability to track fluid flow over space and time. This way, the seismicity triggered by reservoirs impoundment may help to better constrain the relationships between recent observed increases in seismicity and fluid manipulations. Firstly, the volume of water impounded in a reservoir that trigger earthquake is at least one order of magnitude larger than the one reported for injection project (e.g. NRC 2013, McGarr 2014). Secondly, the area explicitly affected by the reservoir impoundments dwarfs the borehole diameter that corresponds to the explicit size of injection perturbation. For both cases, the size of the effective crustal volume where stresses change is driven by the pore-pressure diffusion patterns. Thirdly, the historical time since the onset of pore-pressure changes is much larger for the RTS cases (most reservoir impoundment were operated before the 80' worldwide, e.g. Gupta 2002; Davies et al 2013) than for recently reported fluid injection case studies. This latter point allows the use a larger time window to analyze the time delay and possible long-term patterns between fluid manipulation and seismicity for reservoir than for fluid injection database. Globally there are over 120 sites worldwide where artificial water reservoirs are reported to trigger earthquakes (e.g. Gupta, 2017). Our assumption is that a wide variety of examples of stimulated seismicity can provide independent perspectives regarding the essential problem of the causes of earthquakes (e.g. Simpson, 1986). The mechanism of earthquake triggering by reservoirs involves interaction and coupling between all three of the components for stress changes that are driven by geo-resource production. The weight of the reservoir influences both shear and normal stress at depth. Pore pressure may increase instantly from the compaction of pore space due to the reservoir load and then from the raised water column with a delay due to diffusion. On base of the temporal differences in the response to load and pore pressure, Simpson *et al.* (1988) propose that reservoir-triggered seismicity can be divided into two types: a rapid response related to instantaneous elastic response and a delayed response related to fluid diffusion. When the pressure change at the bottom of a 100 m deep reservoir is 1 MPa, only a small fraction of this stress is propagated to hypocenter depths (e.g. Gough and Gough, 1970; Bell and Nur, 1978 ; Roeloffs, 1988). Under these conditions, a 100 m deep reservoir would thus increases the stress at hypocenter depths by, at most, 0.1 MPa (e.g. Bell and Nur, 1978, Roeloffs, 1988, Deng et al. 2010). This is the same order as the stress changes in simple elastic modeling for earthquake triggering (e.g., Harris, 1998).

In this paper we analyze 20 years of seismicity that follow 26 French reservoir impoundments, in the context of a moderate (1/30 yearly M5 occurrence) tectonic seismicity rate zone. We propose to analyze the reservoir-triggered seismicity in the same framework that the one which is used to describe the tectonic earthquake interactions. Accordingly, we test (L_r), the reservoir length as the equivalent of the mainshock fault length, (which controls the tectonic aftershock triggering rate), as the characteristic reservoir dimension that controls the zone where the stress change induced by reservoir impoundments may trigger seismicity. We analyze the seismicity that is located within 1, 3, 10 L_r-distance from the reservoir in a 20 years window after the impoundment dates. We test 1L_r distance as near field reservoir effect on seismicity, and the 10 L_r-distance as far field null effect of reservoir stress changes on background seismicity, e.g. the seismicity rate is dominated by the tectonic seismicity rate. We compare the results obtained from L_r-distance analysis to the one of 10-30-50 km distance, respectively. In the last section, we aim to extract triggering patterns for seismicity size and time and the possible coupling with reservoir's geometry or local tectonic features.

DATA:

On the French territory there is no mandatory monitoring before and after reservoir impoundments. Accordingly there is no catalogue available from local seismic network around each of the operated reservoirs. In order to robustly analyze the seismicity patterns in the vicinity of reservoir impoundments we are bound to use (Si-Hex) French national earthquake catalogue (Cara et al. 2015). For this catalogue, the completeness value for the magnitude is 2.5 as derived from frequency size distribution (Figure 1). SI-Hex catalogue merges all the available regional seismic arrival times to extract best estimates for both location and magnitudes, within 1962-2009 period (Cara et al. 2015).
The database for reservoirs was built by merging data from hydropower reservoirs and reservoirs related to water supply. The reservoirs are in the top 20 (for either height, or volume, or surface) for the French hydropower reservoir catalogue (http://www.barrages-cfbr.eu/-en-France-.html, see Data and Resources Section). The water-supply reservoirs correspond, in average, to smaller depths for equivalent surfaces than the hydropower reservoirs, respectively (Table 1). For these later, a minimum reservoir surface of 1 km^2 is chosen as a threshold for completeness size. From these databases, volume, depth and surface values of the reservoir lakes are available. Because several of the impoundment dates are much earlier than the 1962 onset for the Si-Hex seismicity catalogue, we further restrict the analysis to the 26 reservoirs that were impounded since 1960 (Figure 2, Table 1).
In term of impoundment time accuracy, the duration for a reservoir impoundment to be completed relies on a minimum of a couple of years. The impoundment date we used, as available data, is the formal date for the onset of reservoir to be operated. It can mismatch by some months the maximum volume or depth of the impounded reservoir. It induces a possible 1year error bar value when tentatively relating the M_{max} or (M_1) first event occurrence to the reservoir impoundment date.
For all reservoirs we estimate the lake length from "google map" open access web based application. The 26 (L_r) reservoir length distribution corresponds to a mean value of 7 km, three-quarters of the reservoir lengths being below the mean value, with only 6 reservoir lengths as L_r > 10km (Table 1). For the 26 reservoirs we analyze, the 10, 30, 50 km distance thresholds we chose correspond to 1.5, 4, 7 averaged values for L_r-distances, respectively.

TECTONIC SETTING

The French metropolitan territory and surrounding areas are part of a continental domain at the western edge of the so-called "stable Europe" domain (Nocquet 2012), belonging to the first-order Eurasian plate. Two micro-plates impact the plate-tectonic context of France, namely the Iberia and Apulia plates (somehow corresponding to Spain and Italy respectively). Although the territory is quite small (typical size of about 1000 km), France and surrounding areas are divided in 4 seismic zones according to the geodynamic contexts (Delouis et al 1993; Cara et al. 2015). The two top seismically active zones (Figure 2) follow the limits of the two micro-plates described above, (i) the Pyrenean mountain range to the Southwest (e.g. Rigo et al. 2010), and (ii) the Western Alpine arc to the Southeast (e.g. Sue et al., 1999). The Northeast zone in geographic continuity with the alpine seismicity is the active Upper Rhine graben system (Figure 2). It is responsible for a significant seismic activity that extends northward through the Lower Rhine system-related seismicity in Belgium and Germany (e.g. Fuhrmann et al., 2013). Last, from the Brittany peninsula to the French Massif Central, there is a diffuse but pervasive seismicity band which develops along a roughly NW-SE elongated

geometry (e.g. Cara et al. 2015).

METHOD

There is no consensus on the a-priori distance-time-size patterns to be selected to relate a given earthquake to a given reservoir impoundment (e.g**.** Gupta, 2002, Klose 2013). From the one hand, some authors suggest, on observational bases, a 30-50 km distances and 10-20 years times from reservoir impoundment to relate an earthquake to a given reservoir (e.g. for a review Gupta, 2002, Klose 2013). These space-time windows question the physics processes that may drive a constant triggering distance to an extended loading source (i.e. not a point source such as a lake surface). The size of the extended sources (i.e. the reservoir lake) ranges on several order of magnitudes in length, surface or volume (e.g. Klose, 2013). From the other hand, there are evidences that the use of the absolute distance captures earthquake-earthquake triggering patterns (as aftershock-mainshock pair) that hide the key properties of the mainshock-aftershock interactions (e.g. Bak et al 2002; Parsons and Velasco, 2009, Tahir et al., 2012, Tahir and Grasso, 2015, de Arcangelis et al 2016). This way, we test in this study the triggering pattern around reservoirs in the continental France using both 10, 30, 50 km and $1L_r$ $3L_r$ $10L_r$ distances as absolute and normalized distances to the reservoirs, respectively.
For tectonic earthquake interactions, the size of the triggering zone is mapped by static stress perturbation. This later is estimated to be in the 1-3 L ranges for aftershocks triggering (Parsons and Velasco 2009; Tahir et al. 2012; Tahir and Grasso, 2015). For the tectonic earthquake analysis (L) is the mainshock fault length as derived from magnitude scale (e.g. Wells and Coppersmith, 1994). In order to mimics the earthquake interaction analysis, we choose in this study (L_r) the reservoir length as the equivalent of the mainshock fault length, the characteristic dimension that drives the stress change pattern induced by reservoir impoundment (e.g. Gupta and Rastogi 1976, Bell and Nur, 1978, Roeloffs, 1988; Deng et al., 2010). Note that the L_r choice, as the larger reservoir dimension, is further sustained by the topology of the French Alps reservoir, which are strongly elongated due to alpine valley geomorphology. When the reservoir depth controls the stress change value, Gupta (1985), Grasso and Sornette (1998) reported the water depth does not control the M_{max} size. Similar observations are reported for the tectonic earthquake triggering where the aftershock productivity and location are driven by the size of the earthquake trigger rather than by its stress drop values, respectively (e.g. Helmstetter, 2003; de Arcangelis et al. 2016). These observations suggest that the area where the stress change is applied is more important than the maximum stress value to understand earthquake triggering. This way the volumetric stress changes induced by the reservoir impoundment mimic the stress change induced by each of the tectonic earthquakes. The analysis we proposed in this study, that uses L_r distance to estimate triggering patterns, is this way equivalent to consider the reservoir impoundment as an earthquake mainshock, the (RTS) reservoir triggered seismicity being the corresponding aftershocks. The choice of the L_r normalized distance to reservoir allows us to test how the reservoir size possibly impacts both the triggering efficiency and the M_{max} value in the context of RTS. Such methodology is suggested for different anthropogenic seismicity types (e.g. McGarr et al., 2002; De Arcangelis et al., 2016). It was recently tested on several waste-water injection case studies (e.g. NRC 2013, McGarr 2014; Dietrich et al., 2015; Elst et al., 2016).
Using the L_r and km triggering thresholds, we further investigate the possible interrelations between the reservoir dimensions (volume, surface, length, depth) and the earthquake patterns (M_{max}, number, time delay). We define RTS as earthquake sequence that occurs within 1 L_r and 10 km from the reservoir in a 20 years time window after impoundment

time. We test 1 L_r-distance as robust near field reservoir effect, and 10 L_r-distances as distances with null effect from reservoir induced stress changes on seismicity, respectively. For time analysis, the completeness in the seismicity catalogue (robust since 1962, (Figure 1), and the impoundment date distribution, (1959-1995, Table (1)), do not allow to robustly compare pre-impoundment and post-impoundment seismicity for each of the case studies.

RESULTS

1. Average patterns for Reservoir Triggered Seismicity

To stay away from specific case study and in order to smooth on fluctuations due to single event analysis, we used superposed epoch analysis for the time series after the 26 reservoir impoundment dates (e.g. Colllombet et al., 2003; Singh, 2006; Lemarchand and Grasso, 2007; Schmid and Grasso, 2012, Parsons et al. 2017). The superposed epoch is constructed via a table with one row for each impoundment years (26 rows of key events, since our study deals with 26 reservoirs) and 10 columns containing the number of possibly triggered events for the impoundment and subsequent years (2-year bin) and for the 20 years after this key event. The triggered seismicity is designated for the 1-3-10 L_r and the 10-30-50 km distance ranges. The superposed epoch is the stacking of the number of triggered events in each column. The stacked time series are presented using a common (t_0) for the 26 impoundment times (Figure 3-4). To assess the statistical significance of the patterns that emerged from the superposition, we applied Monte Carlo techniques (e.g. Kelly and Sear, 1984; Lemarchand and Grasso, 2007, Tahir et al. 2012) involving 1000 random sets of key events. It is assessed by sampling at random with replacement (bootstrap procedure) 1000 sets of 26 impoundment dates from the impoundment time series ("synthetic impoundment years"). Each 26 synthetic impoundment date in a set is assigned a location picked up randomly from the list of reservoir ("synthetic reservoir location"). The length distribution of the 26 real reservoirs is tacked onto each synthetic set. Accordingly the synthetic reservoirs share the same variability in location time and length domains than the original series. The 1000 sets of 26 synthetic reservoirs are then analyzed in the same manner as the real reservoir set to assess the confidence levels for the superposed epoch values.

We observed that, within 1L_r-distance from the reservoirs, the real seismicity rate increases significantly above the tectonic fluctuations twice, i.e. in the 0-2yrs and 4-6 years after impoundment time (Figure 3). For 3L_r-distance, only the peak of activity in the 0-2yrs is accepted at a 95% confidence level (Figure 3). Note that the synthetic and the stacked time series overlap, for the largest distances. It supports the seismicity we observed within the 10L_r-distance is characteristic of the tectonic rate values**.** For the km distance analysis, only the peak of activity in the 0-2yrs exceeded the upper 95% confidence limit for 10 and 30 km distances (Figure 4). Accordingly, the seismicity rates within 1L_r and 10-30 km distances all peak up within 2 years from the impoundment dates. This pattern agrees with previous observations of the short time and short distance triggering for type #1 RTS seismicity (e.g. Simpson et al 1988, Ibenbrahim et al. 1989).

These patterns are also recovered when reshuffling impoundment time or reservoir length for the reservoir we uses. All these tests support there is significant increase in seismicity rate within 1L_r-distance after reservoir impoundments.

To be able to compare the seismicity rate values for different triggering distances, we normalize the rate by the distance ranges we used. This way, the normalized peak density in 3L_r-distance is of the order of 4.5 event/L^2 during the first 2 years, i.e. two times less than the one in 1L_r-distance. These values support a decrease within 1-3 L_r-distance to reservoir of the triggered seismicity rate relatively to impoundment times**.** Note the far field tectonic

rate, which is estimated by average density in $10L_r$, is the order of 1.0 event/L^2. These responses to reservoir loading mimic the damage relaxation reported after both tectonic mainshock and others anthropogenic seismicity types (e.g. Dietrich et al. 2015). For the seismicity rate around continental French reservoirs, the low number of events inhibits to qualify the decrease over time of seismicity rate as either a power or an exponential law (e.g. Mignan, 2015).

2. Triggering efficiency, M_{max} and reservoir dimensions:

Six out of the 26 artificial lakes we analyze triggered seismicity within 1 L_r, 11 within 3 L_r, 22 within 10 L_r-distances from the reservoir, respectively (Table 1, 2). Five over six of the reservoirs that trigger earthquakes in 1 L_r-distance are in the top 5 for reservoir lengths (Figure 5, Table 1). The statistical significance of the reservoir length difference between 1 L_r trigger reservoirs and the others ones is robust as tested using the Wilcoxon-Mann-Whitney (WMW) test (Wilcoxon, 1945; Mann & Whitney, 1947). This test compares medians and/or distributions, under the assumption that the shapes of the distributions are the same between the groups. Using the WMW test, the lengths of reservoirs that trigger in 1-3 L_r and 10-30 km distances are significantly larger than the lengths of other reservoirs (Table 2). These results support (i) we need long enough reservoirs to be able to trigger earthquake; (ii) the robust reservoir triggered earthquakes are bounded to be located in the reservoir near field. For those reservoirs that trigger in 1 L_r the M_{max} values are in the 2.7-4.7 magnitude and 0-25 km distance ranges (Table 1; Figure 6); (iii) The seismicity that emerges as triggered in 10 L_r-distances, and observed for the four-fifths of the reservoirs, corresponds to the tectonic seismicity background.

To quantify the role of the reservoir dimensions as a control parameter for seismicity triggering we use the framework of detection and prediction methodology (i.e. success rate, false alarm rate, failure to predict (e.g. Molchan,1997, de Arcangelis et al., 2016)). We aim to delimit the domain in the length, volume, surface and depth space that optimally isolates the earthquake trigger reservoir. In such a framework, the success rate is defined as the rate of $1L_r$ trigger reservoir within the imposed dimension domain, e.g. threshold values on Length and Volume dimensions (Figure 7). The false alarm rate is defined as the number of 10 L_r earthquakes within the same domain than the one previously imposed, e.g. threshold values on Length and Volume dimensions (Figure 7). For robustness we further ranked earthquake that occurred within $3L_r$-distance, and that fit the selected Length-Volume domain as blank results.

As example, $L_r > 8$ km and $V > 210\ 10^6\ m^3$ together capture more than 5/6 out of $1L_r$ trigger reservoirs. This corresponds to 5/6 successes, including 1 reservoir in $3L_r$ distance as a blank event (Figure 7). To be able to recover the same success rate for km-distance performance, (i.e. 7/9 trigger reservoirs within 10 km distance), we must include 2 false alarms and 5 blank distances, i.e. 7 reservoirs that do not trigger in 10 km distances (Figure A1). Accordingly, the volume-length pair for the triggering within $1L_r$-distance range is the more efficient to capture trigger reservoirs, as estimated by both success and false alarm rates. When considering the length dimension solely, the $L_r > 8$ km threshold captures 5/6 triggers in 1 L_r-distance without either blank or false alarm occurrence (Figure 7, Table 3). To access to the same (5/6) success rate for 1 L_r trigger, using volume dimension alone, we need to involve 2 false alarms. In comparison, using 10 km distance to isolate seismic trigger reservoir without false alarm and blank event, we resolve, (for $L_r > 18$ km or $V>1000\ 10^6\ m^3$), 3/9 or 1/9 success, respectively (Table 3; Figure A1).). Within this framework, the length dimension is more efficient to extract near field triggering than depth or volume or surface for reservoir dimension (Figure 7, Table 3).

When numerous rankings to select the best reservoir proxy to estimate seismicity triggering are possible, the ones based on the distance normalized by reservoir length rather than absolute distance to reservoir emerge as the best thresholds in term of false alarm rates and failure to predict rates (e.g. for quantifying prediction skills, Molchan (1990, 1997); Grasso and Zaliapin, (2004), Schmid et al. (2012), De Arcangelis et al. (2016)).

3. Time analyses for M_{max} occurrence:

When focusing on time analysis for M_{max} occurrence, we find most of the largest magnitudes to occur within 7 years from the reservoir impoundment date, for both 1 L_r and 10 km trigger reservoirs (Figure 8). For 1 L_r trigger reservoirs, a single late M_{max} event occurred 17 years after a reservoir impounded. Apart from the 1 L_r -10 km near field and 7 years short time triggered event, a second type of large triggered shock possibly correspond to RTS that is delayed in space and time (3 L_r -30 km, 10-15 years) relatively to the reservoir impoundments (Figure 8). These patterns fit the late RTS response to reservoir impoundment as classified by Simpson et al. (1988). These authors suggest the earliest events (close to the reservoir in time and space) to fit a mechanical response to the vertical stress change due to reservoir mass loading, whereas the second, delayed, type is suggested to be driven by pore-pressure diffusion over time and space. For the database we work with, we do not resolve a large gap, ($\Delta t<3$yrs), between (M_1) the first event of the sequence and the M_{max} events, for all 1 L_r-trigger reservoirs (Figure 8**).** It supports that M_{max} earthquakes are not part of long lasting seismic swarms on our studied sites.

DISCUSSION

We analyze the seismicity patterns in the vicinity of the top 26 largest French reservoirs. Because a comprehensive seismic catalogue (Sis-Hex, Mc>2.5 1962-2009) is only available since 1962, we select reservoir impounded within the 1959-1995 period in order to be able to analyze the seismicity in a 20-year time window after the reservoir impoundments. Accordingly we aim toward characterizing seismicity patterns around reservoirs that will help to classify seismicity as either (RTS) Reservoir Triggered Seismicity or as tectonic seismicity. Similarly to earthquake interaction analysis (e.g. Lemarchand and Grasso, 2006; Tahir and Grasso 2015, De arcangelis et al. 2016), we test (L_r) the reservoir length (the equivalent of a mainshock fault length), as the characteristic dimension that drives the stress change pattern induced by reservoir impoundments. Such a working hypothesis corresponds to test how the reservoir size possibly impacts on the reservoir triggering efficiency and on the M_{max} value of reservoir triggered seismicity. The reference we used, for tectonic seismicity background (i.e. the far field seismicity not related to reservoir impoundment), is the seismicity within 10 L_r or 50 km distances from the reservoir. We summarize below how the triggering patterns, in each of the time and space and, size domains help to discriminate triggered seismicity within either L_r normalized or absolute distance to reservoirs, respectively.

Observed French reservoir seismicity and previously referenced French RTS case studies

On the 6 lake reservoirs we identified as triggering in 1L_r distance, 4 case studies (Vouglans, Granval, Ste-Croix, Monteynard) correspond to previously referenced RTS cases. For the Serre-Poncon and Caramany reservoirs, we suspect the small M_{max}=2.7-3.3 values in 1L_r distance is the main reason for these case studies not to be reported as RTS case (e.g. Gupta 2002; Davies et al. 2013). Except for the one Caramany case, located in Eastern Pyrenees (Figure 9), each of the dams that trigger within 1L_r-distance are ranked in the top 3 French reservoirs for at least one of the reservoir dimension values (Table 4).

To further constrain the triggering/non-triggering pattern we observed using national earthquake catalogue, it is worth to mention the 2 negative, and one positive, evidences for reservoir triggered seismicity that are resolved by observations from local seismic monitoring. In the case of Grand-Maison and Mt-Cenis reservoir impoundments (Table 1), local seismic networks deployed before impoundment did not resolved any change in seismicity before and after impoundment time, respectively (Plichon et al., 1979; Hatzfeld, 1992). Similarly, on these two sites we do not resolved triggering in $1L_r$ distance, 20 years time, using the French national earthquake catalogue (Table 1).
Using data from a temporary seismic network, the one positive evidence for M<2 increase in seismicity rate (i.e. below the resolution of the French national catalogue we used) is reported for Sainte-Croix reservoir, contemporary to the first reservoir impoundment, (Plichon et al., 1979). From our analysis, the Sainte-Croix reservoir also corresponds to seismicity triggering within 1 L_r-distance (Table 1, 4). These local studies confirm the non-trigger/trigger reservoir type we identify using M2.5 seismicity catalogue.

L_r versus km triggering distance to reservoirs:
We find that a quarter of the reservoirs (6 reservoir dams) trigger seismicity within 1Lr-20 years space-time window and 9 reservoirs (one third) trigger within 10 km distances.
The comparison between the superposed epoch analysis and synthetic random series points on (i) the 10 L_r or 50 km distance seismicity to be similar to the tectonic seismicity; (ii) the seismicity rates after reservoir impoundment are significantly larger, within 1 L_r-distance than the one expected from tectonic seismicity, up to 6 years after impoundment (Figure 3).
The reservoirs that trigger in the near field distance are larger as estimated by length values than the non-triggering ones, both for triggering in 1-3L_r and 10-30 km distances (Table 2).
One must note that the seismicity rate values within 3 L_r, 30 km are still dominated by the longest reservoirs, i.e. the ones that trigger in 1 L_r – 10 km distance. The seismicity for these long length reservoirs contributes to 90% of the stacked seismicity rate values, in the 3 Lr-distances. Also of the 6 reservoirs, that trigger M2.7-4.6 earthquakes within 1 Lr distance, are the ones that trigger the largest events, M4.2-4.7, within 3L_r-distances (Figure 7).
In an attempt to extract thresholds to relate near field seismicity triggering to reservoir dimensions, length-volume pair is the best proxy to isolate triggering in $1L_r$ distance (Figure 7, Table 3). This reservoir dimension pair minimizes the false detection rate (i.e. a reservoir dimension within the requested range of dimension values but with no seismicity in $1L_r$). For L_r normalized distance, Length-Volume pair allows for a 80% detection success, with one false detection. It outperforms the km distance results (30% of detection success, 6 false detections). Using solely a (L_r) length threshold allows to extract 5/6 (80%) of 1Lr triggers without false detections (Table 3, Figure 7). To achieve such the same 80% success rate for triggers in the 10 km distances, it requests 14 false detections (Figure A1). When imposing no false detection, L_r threshold for 10 km distance corresponds to 33% of detection success, solely (Figure A1). These results support that it is more difficult to define efficient thresholds for triggering seismicity using absolute rather than normalized distance from reservoirs, respectively.
We do not find any correlation between reservoir dimensions (e.g. Gupta 1985) and the observed 2.7-4.6 range of M_{max} values. It supports a non-deterministic triggering for M_{max} as proposed for others type of anthropogenic seismicity. This way the RTS is reminiscent of the natural tectonics seismicity, where the slow driving for stress changes is known (i.e. the plate tectonic plate and reservoir impoundment, respectively), and the M_{max} values correspond to random "draws" in a Gutenberg-Richter distribution (e.g. Helmstetter et al., 2002, de Arcangelis et al., 2016; Elst et al., 2016).

Trigger reservoirs and geo-mechanical setting

Beyond the analysis of interrelations between reservoir dimensions and reservoir triggering patterns, we also try to sort out which specificities in tectonics setting, if any, are candidates to enhance the susceptibility to seismic slip instabilities as observed as RTS.

The French seismicity is sorted as 4 seismic zones, the Pyrenean range, the western alpine arc, the Rhine Graben, and the Massif Central - Brittany diffuse strip (e.g. Cara et al. 2015). The 6 trigger reservoirs we identify are located as (4) Western Alpine Arc, (1) Pyrenean range, (1) Massif Central (Figure 9). Whereas the Alps and Pyrenees zone are described as active mountain belts and microplate boundaries (Metois et al., 2015; Rigo et al., 2015), there is no reported value for the vanishingly small deformation of Massif Central - Brittany zone (Tesauro et al, 2006).

The current tectonic stress regime in the external Alps context is regionally admitted as a strike-slip regime (σ_1, σ_3 being S_H and S_h respectively, e.g. Sue et al 1999, 2007; Delacou et al., 2004). This stress field orientation does not promote a direct loading effect of the reservoir impoundment to move the Mohr-Coulomb circle toward slip instabilities (e.g. Grasso and Sornette 1998). Nonetheless the Monteynard and Vouglans reservoirs, which triggered M4.5 normal faulting and strike-slip earthquakes within 2 years from impoundment (e.g. Grasso et al. 1992, Grellet et al., 1993) as genuine RTS type #1 (short time, short distance from the reservoir loading, e.g. Simpson et al. 1986). Such patterns are recovered for the Caramany, Eastern Pyrenees case, as a fast response to loading in a strike slip regime setting (e.g. Rigo et al., 2010; 2015).

For the others reservoirs, we observed smaller and delayed shocks (M3, 8-15 years), for Serre-Ponçon and Sainte Croix reservoirs (South Alps) and Grandval reservoir in Massif Central (Figure 9, Table 1, 4). This change in time delay for M_{max} may be tentatively related to permeability changes between (i) the highly fractured sedimentary layers that dominate the shallow structures of external Alps where fast RTS type #1 responses are located (e.g. Grasso et al. 1992) and (ii) the low permeability granite rocks that characterize the Hercynian Massif-Central zone. The overall seismicity of the Massif-Central Brittany zone, as organized along a diffuse NW-SE zone, corresponds to major 360 Ma year old shear zone structure in the Variscan crust. This intraplate seismic activity bears witness of the major role played by old inherited structures in terms of current seismicity. This seismicity located far away from the deforming areas (Alps, Pyrenees) rises up the questions of stress transfers within the crust, the distance to critical thresholds for slip instabilities and the related earthquake triggering processes (e.g. Grasso and Sornette, 1998). These observations in different tectonic settings may suggest the RTS values are somewhat bounded by the background seismicity patterns

Conceptual model for reservoir seismicity triggering

Overall, our analyses of earthquake triggering around French reservoirs in time and space domains point on the recurrent importance of L_r analysis versus km distance analysis. It supports the reservoir influence zone (infiltrated volume) scales with lake size rather than simple distance to a local "point source" load, especially in the reservoir near field (e.g. Ibenbrahim et al. 1989).

We suggest the reservoir impoundment impacts the upper crust the same way the earthquake slip changes the upper crust stresses. The surface reservoir load modifies the state of stress, specifically the vertical stress and the effective stresses through pore pressure changes, in an area that scales with L_r, the reservoir length. Similarly to earthquake interaction, our study suggests the size of the surface where the stresses change is more

important than the maximum stress change value in order to control both the number of reservoir triggered earthquakes as well as their M_{max} values (e.g. Grasso and Sornette, 1998; McGarr et al., 2002; de Arcangelis et al. 2016; Elst et al. 2016).
This way, our results support the RTS to be analyzed as the aftershocks of the reservoir loading, this later being a mechanical analog to a slow earthquake loading (Table 5). This conceptual model was suggested to apply for seismicity induced by fluid injection (e.g. Dieterich et al. 2015). It gives clue to possibly constrain M_{max} value for RIS as driven by reservoir-size magnitude equivalent. This constrain can either apply as a deterministic constrain (e.g. McGarr, 2014; McGarr et al., 2015), with injected volume that is suggested to scale with the M_{max} value for wastewater disposal) or as a stochastic one (e.g. De Arcangelis et al. 2016, Elst et al., 2016). To push further the analogy between RTS and aftershock sequence, we surmise from Figure (10) the (M_{theo}) theoretical maximum size for the RTS relatively to a probable trigger reservoir of (L_r) length, to be estimated by,

$$<M_{theo}> = M^*_{reservoir} - \alpha \quad (1)$$

with $M^*_{reservoir} = M(L_r)$, L_r being the reservoir length and $M^*_{reservoir}$ is the reservoir magnitude equivalent. $M(L_r)$ is estimated using an empirical magnitude fault length relationship (e.g. Wells and Coppersmith 1994). α-value is an a-priori constant value and $<M_{theo}>$ denotes the mean M_{theo} value. On Figure (10) all observed M_{max}values are smaller than $M^*_{reservoir}$ values, supporting $M_{theo} < M^*_{reservoir}$. The equation (1) is the equivalent of the Bath law for the average largest aftershock size (e.g. Bath, 1951; Tahir et al. 2012, De Arcangelis et al. 2016). For French reservoirs we find $\alpha = 2.6$ +/- 1.0 for $1L_r$, M_{max} events. It is to say the M_{theo} for RIS is weaker than the one expected from the aftershock Bath law, where $\alpha = 1.2$ +/- 0.5 for worldwide seismicity (e.g. Tahir et al. 2015). From a practical way, our results allow to propose empirical bounds to the RTS-M_{max} values as soon as the reservoir construction is planned, i.e. $M^*_{reservoir} = M(L_r)$ is known. Ongoing analyses will try to constrain how a change in α – value is possibly observed regionally as controlled by the faulting style (i.e. the tectonic setting, Tahir et al 2015) or the earthquake stress drops (Wetzler et al. 2016), as suggested for tectonic earthquakes.

Conclusion:

The analysis of seismicity in the neighborhood of the 26 largest French reservoirs (impounded in the 1959-1995 period) supports that 6-9 reservoirs trigger earthquakes within $1L_r$-10km distances from the reservoirs, respectively. Using L_r distance to reservoir, (L_r being the reservoir lake length), as a characteristic distance for the reservoir impact on seismicity, shows that seismicity rate within $1L_r$-$3L_r$ and 2 years from reservoir impoundment is robustly larger than the one expected from randomized regional tectonic seismicity. Furthermore the trigger reservoirs in $1L_r$ distances are robustly larger in L_r-values than the non-triggering reservoirs. All these analyzes validate the $1L_r$ distance threshold as the influence zone, where stress and pore pressure changes due to reservoir impoundment drive the seismicity triggering. It suggests L_r to be a control parameter for RTS. When sorting all reservoir dimensions, L_r outperformed volume, depth or surface dimension to isolate trigger versus non-trigger reservoirs.
For near field interactions between the tectonic mainshock and aftershocks, the size of the triggering zone is mapped by the static stress perturbations due to the mainshock slip. Similarly, our results suggest RTS is located within the (1-3L_r) near field distances from reservoirs. By comparison, the seismicity located at $10L_r$-distance from reservoirs, corresponds to the far field tectonic seismicity background. In such a context, our results

support RTS and reservoir impoundment to be analog to aftershocks and a slow main-shock, respectively. For all the reservoirs we analyzed when the triggered seismicity patterns is driven by the largest L_r values, we failed to identify any deterministic control parameter for M_{max} values as a function of the reservoir geometry (volume, surface, length, depth). Alternatively, from a practical point of view, our results suggest empirical bounds to the RTS-M_{max} values that are in average smaller than the reservoir magnitude equivalent as $M_{(theo)} < M^*_{reservoir}$, with $M^*_{reservoir} = M(L_r)$, the reservoir magnitude equivalent.

Data and Resources:

- Earthquake catalogue is from http://www.franceseisme.fr/sismicite.html (latest access on January 20th 2017)). The comprehensive technical description is in Cara et al., (2015)
- Location and length of reservoir dam and reservoir lake were searched using "Google map" service, (latest accessed on January 20th, 2017)
- Reservoir dimensions and impoundment date database for electric power dam was searched using http://www.barrages-cfbr.eu/-en-France-.html, (latest accessed on January 20th , 2017). Information for others reservoirs are extracted from https://fr.wikipedia.org/wiki/Liste_des_plus_grands_lacs_et_%C3%A9tangs_de_France#.C3.89tendues_d.27eau_artificielles, (latest accessed on January 20th , 2017).
- All other data used in this paper came from published sources listed in the references.

Acknowledgments: A.K. was supported by a grant from the EPOS-IP Anthropogenic Hazard EC H2020 project (*EPOS IP. Project* ID: 676564). J.-R.G. contribution was partially supported by EPOS-IP (Anthropogenic Hazard) and SERA EC-H2020, (*SERA. Project* ID: 730900) projects. The data are also available through the EPOS-IP platform. Discussions with partners of the EPOS-Anthropogenic Hazard group motivated the study.

References :

Atkinson, G. M., Eaton, D. W., Ghofrani, H., Walker, D., Cheadle, B., Schultz, R., ... & Liu, Y. (2016). Hydraulic fracturing and seismicity in the Western Canada Sedimentary Basin. *Seismological Research Letters*, *87*(3), 631-647.

De Arcangelis, L., Godano, C., Grasso, J. R., & Lippiello, E. (2016). Statistical physics approach to earthquake occurrence and forecasting. *Physics Reports*, *628*, 1-91.

Bak, P., Christensen, K., Danon, L., & Scanlon, T. (2002). Unified scaling law for earthquakes. *Physical Review Letters*, *88*(17), 178501.

Båth, M. (1965), Lateral inhomogeneities of the upper mantle, Tectonophy- sics, 2(6), 483–514.

Bell, M. L., & Nur, A. (1978). Strength changes due to reservoir-induced pore pressure and stresses and application to Lake Oroville. *Journal of Geophysical Research: Solid Earth*, *83*(B9), 4469-4483.

Cara, M., Cansi, Y., Schlupp, A., Arroucau, P., Béthoux, N., Beucler, E., ... & Delouis, B. (2015). SI-Hex: a new catalogue of instrumental seismicity for metropolitan France. *Bulletin de la Société Géologique de France*, *186*(1), 3-19.

Collombet, M., Grasso, J. R., & Ferrazzini, V. (2003). Seismicity rate before eruptions on Piton de la Fournaise volcano: Implications for eruption dynamics. *Geophysical research letters*, *30*(21).

Davies, R., Foulger, G., Bindley, A., & Styles, P. (2013). Induced seismicity and hydraulic fracturing for the recovery of hydrocarbons. *Marine and Petroleum Geology*, *45*, 171-185.

Delacou, B., Sue, C., Champagnac, J. D., & Burkhard, M. (2004). Present-day geodynamics in the bend of the western and central Alps as constrained by earthquake analysis. *Geophysical Journal International*, *158*(2), 753-774.

Delouis, B., Haessler, H., Cisternas, A., & Rivera, L. (1993). Stress tensor determination in France and neighbouring regions. *Tectonophysics*, *221*(3-4), 413-438.

Deng, K., Zhou, S., Wang, R., Robinson, R., Zhao, C., & Cheng, W. (2010). Evidence that the 2008 Mw 7.9 Wenchuan earthquake could not have been induced by the Zipingpu Reservoir. *Bulletin of the Seismological Society of America*, *100*(5B), 2805-2814.

Dieterich, J. H., Richards-Dinger, K. B., & Kroll, K. A. (2015). Modeling injection-induced seismicity with the physics-based earthquake simulator RSQSim. *Seismological Research Letters*.

Ellsworth, W. L., (2013). Injection-induced earthquakes. *Science*, *341*(6142), 1225942.

Elst, N. J., Page, M. T., Weiser, D. A., Goebel, T. H., & Hosseini, S. M. (2016). Induced earthquake magnitudes are as large as (statistically) expected. *Journal of Geophysical Research: Solid Earth*, *121*(6), 4575-4590.

Fuhrmann, T., Heck, B., Knöpfler, A., Masson, F., Mayer, M., Ulrich, P., ... & Zippelt, K. (2013). Recent surface displacements in the Upper Rhine Graben—preliminary results from geodetic networks. *Tectonophysics*, *602*, 300-315.

Gough, D. I., & Gough, W. I. (1970). Load-induced Earthquakes at Lake Kariba–II. *Geophysical Journal International*, *21*(1), 79-101.

Grellet, B., Combes, P., Granier, T. et Philip, H. (1993) - Sismotectonique de la France métropolitaine dans son cadre géologique et géophysique. *Mém. Soc. Géol. Fr.* n°164, 75 p.

Grasso, J.-R., & Sornette, D. (1998). Testing self-organized criticality by induced seismicity. *Journal of Geophysical Research: Solid Earth*, *103*(B12), 29965-29987.

Grasso, J.-R., Guyoton, F., Fréchet, J., & Gamond, J. F. (1992). Triggered earthquakes as stress gauge: Implication for the uppercrust behavior in the Grenoble area, France. *pure and applied geophysics*, *139*(3), 579-605.

Grasso, J.-R., & Zaliapin, I. (2004). Predictability of volcano eruption: lessons from a basaltic effusive volcano. *Geophysical research letters*, *31*(5).

Gupta, H. K. (1985). The present status of reservoir induced seismicity investigations with special emphasis on Koyna earthquakes. *Tectonophysics*, *118*(3-4), 257-279.

Gupta, H. K. (2002). A review of recent studies of triggered earthquakes by artificial water reservoirs with special emphasis on earthquakes in Koyna, India. *Earth-Science Reviews*, *58*(3), 279-310.

Gupta, H. K. (2017). Continued Reservoir Triggered Seismicity at Koyna, India, 2nd, Induced Seismicity Workshop, Abstract book, Schatzalp, 14-17, March 2017.

Gupta, H. K., & Rastogi, B. K. (1976). Dams and earthquakes. In *Developments in geotechnical engineering* (No. 11). Elsevier Scientific Pub. Co.

Harris, R. A. (1998). Introduction to special section: Stress triggers, stress shadows, and implications for seismic hazard. *Journal of Geophysical Research: Solid Earth*, *103*(B10), 24347-24358.

Hatzfeld, D. 1992, Sismicity monitoring around the Grand-maison reservoir, 1986-1990, final report EDF-LGIT OSUG report, 60p.

Helmstetter, A. (2003). Is earthquake triggering driven by small earthquakes?. *Physical Review Letters*, *91*(5), 058501.

Ibenbrahim, A., Ni, J., Salyards, S., & Ali, I. M. (1989). Induced seismicity of the Tarbela reservoir, Pakistan. *Seismological Research Letters*, *60*(4), 185-197.

Kelly, P. M., & Sear, C. B. (1984). Climatic impact of explosive volcanic eruptions. *Nature*, *311*(5988), 740-743.

Klose, C. D. (2013). Mechanical and statistical evidence of the causality of human-made mass shifts on the Earth's upper crust and the occurrence of earthquakes. *Journal of Seismology*, *17*(1), 109-135.

Lemarchand, N., & Grasso, J. R. (2007). Interactions between earthquakes and volcano activity. *Geophysical Research Letters*, *34*(24).

Mann, H. B., & Whitney, D. R. (1947). On a test of whether one of two random variables is stochastically larger than the other. *The annals of mathematical statistics*, 50-60.

McGarr, A. (2014). Maximum magnitude earthquakes induced by fluid injection. *Journal of Geophysical Research: solid earth*, *119*(2), 1008-1019.

McGarr, A., Simpson, D., & Seeber, L. (2002). Case histories of induced and triggered seismicity. *International Geophysics Series*, *81*(A), 647-664.

McGarr, A., Bekins, B., Burkardt, N., Dewey, J., Earle, P., Ellsworth, W., ... & Rubinstein, J. (2015). Coping with earthquakes induced by fluid injection. *Science*, *347*(6224), 830-831.

Metois, M., D'Agostino, N., Avallone, A., Chamot-Rooke, N., Rabaute, A., Duni, L., ... & Georgiev, I. (2015). Insights on continental collisional processes from GPS data: Dynamics of the peri-Adriatic belts. Journal of Geophysical Research: Solid Earth, 120(12), 8701-8719.

Mignan, A. (2015). Modeling aftershocks as a stretched exponential relaxation. *Geophysical Research Letters*, *42*(22), 9726-9732.

Molchan, G. M. (1990). Strategies in strong earthquake prediction. *Physics of the Earth and Planetary Interiors*, *61*(1-2), 84-98

Molchan, G. M. (1997). Earthquake prediction as a decision-making problem. *Pure and Applied Geophysics*, *149*(1), 233-247.

National Research Council. (2013). *Induced Seismicity Potential in Energy Technologies*. Washington, DC: The National Academies Press. https://doi.org/10.17226/13355.

Nawaz, M. A., & Curtis, A. (2016). Bayesian inversion of seismic attributes for geological facies using a Hidden Markov Model. *Geophysical Journal International*, ggw411.

Nocquet, J. M. (2012). Present-day kinematics of the Mediterranean: A comprehensive overview of GPS results. *Tectonophysics*, *579*, 220-242.

Parsons, T., and A. A. Velasco (2009), On near-source earthquake triggering, J. Geophys. Res., 114, B10307, doi:10.1029/2008JB006277.

Parsons, T., Malagnini, L., & Akinci, A. (2017). Nucleation speed limit on remote fluid-induced earthquakes. *Science advances*, *3*(8), e1700660.

Plichon, J.N., P. Gevin, Hong Trong Pho, P. Londe, P. Petteville, (1979), Seismicity of large reservoirs, Trans., Proc., 13th Congress on Large Dams, New Delhi, India, 1346-1362.

Rigo, A. (2010). Precursors and fluid flows in the case of the 1996, M L= 5.2 Saint-Paul-de-Fenouillet earthquake (Pyrenees, France): A complete pre-, co-and post-seismic scenario. *Tectonophysics*, *480*(1), 109-118.

Rigo, A., Vernant, P., Feigl, K. L., Goula, X., Khazaradze, G., Talaya, J., ... & Sylvander, M. (2015). Present-day deformation of the Pyrenees revealed by GPS surveying and earthquake focal mechanisms until 2011. *Geophysical Journal International*, *201*(2), 947-964.

Roeloffs, E. A. (1988). Fault stability changes induced beneath a reservoir with cyclic variations in water level. *Journal of Geophysical Research: Solid Earth*, *93*(B3), 2107-2124.

Schmid, A., & Grasso, J. R. (2012). Omori law for eruption foreshocks and aftershocks. *Journal of Geophysical Research: Solid Earth*, *117*(B7).

Simpson, D. W. (1986). Triggered earthquakes. *Annual Review of Earth and Planetary Sciences*, *14*(1), 21-42.

Simpson, D. W., Leith, W. S., & Scholz, C. H. (1988). Two types of reservoir-induced seismicity. *Bulletin of the Seismological Society of America*, *78*(6), 2025-2040.

Singh, Y. P. (2006). Statistical considerations in superposed epoch analysis and its applications in space research. Journal of atmospheric and solar-terrestrial physics, 68(7), 803-813

Sue, C., Thouvenot, F., Fréchet, J., & Tricart, P. (1999). Widespread extension in the core of the western Alps revealed by earthquake analysis. Journal of Geophysical Research: Solid Earth, 104(B11), 25611-25622.

Sue, C., Delacou, B., Champagnac, J. D., Allanic, C., Tricart, P., & Burkhard, M. (2007). Extensional neotectonics around the bend of the Western/Central Alps: an overview. *International Journal of Earth Sciences*, *96*(6), 1101-1129.

Tahir, M., Grasso, J. R., & Amorèse, D. (2012). The largest aftershock: How strong, how far away, how delayed?. *Geophysical Research Letters*, *39*(4).

Tahir, M., & Grasso, J. R. (2015). Faulting style controls for the space–time aftershock patterns. *Bulletin of the Seismological Society of America*.

Tesauro, M., Hollenstein, C., Egli, R., Geiger, A., & Kahle, H. G. (2006). Analysis of central western Europe deformation using GPS and seismic data. *Journal of Geodynamics*, *42*(4), 194-209.

van der Elst, N. J., Savage, H. M., Keranen, K. M., & Abers, G. A. (2013). Enhanced remote earthquake triggering at fluid-injection sites in the midwestern United States. *Science*, *341*(6142), 164-167.

Wells, D. L., & Coppersmith, K. J. (1994). New empirical relationships among magnitude, rupture length, rupture width, rupture area, and surface displacement. *Bulletin of the seismological Society of America*, *84*(4), 974-1002.

Wetzler, N., Brodsky, E. E., & Lay, T. (2016). Regional and stress drop effects on aftershock productivity of large megathrust earthquakes. *Geophysical Research Letters*, *43*(23).

Wilcoxon, F. (1945). Individual comparisons by ranking methods. *Biometrics bulletin*, *1*(6), 80-83.

Table

a)

Reservoir type	N	Name	Latitude[°]	Longitude[°]	Length[km]	Impoundmt[year]	Surface[km²]	Depth[m]	Volume[10^6 m³]	CumN[1L]	CumN[3L]	CumN[10L]	CumN[10km]	CumN[30km]	CumN[50km]	Mmax[1L]	Mmax[3L]	Mmax[10L]	Mmax[10km]	Mmax[30km]	Mmax[50km]
Hydropower	1	Grandval	44.92	3.07	25	1959	11	79	271	6	14	144	1	6	8	2.9	3.6	5.5	2.7	2.9	2.9
Hydropower	2	Serre-Ponçon	44.47	6.27	18	1961	28.2	90	1270	7	34	224	3	13	26	2.7	4.2	5.5	2.7	3.2	4.2
Hydropower	3	Monteynard-Avignonet	44.95	5.68	9	1962	6.57	115	309	5	22	72	5	24	30	4.6	4.6	5.5	4.6	5.5	5.5
Hydropower	4	Vouglans	46.38	5.67	27	1969	16	100	592	7	29	427	2	6	10	4.6	4.6	4.6	4.6	4.6	4.6
Hydropower	5	Sainte-Croix	43.73	6.13	16	1975	22	93	767	1	12	274	%%	5	13	2.8	4	4.3	%%	4	4
Water-supply	6	Caramany	42.73	2.55	5	1995	1.8	57	26	4	17	39	17	21	39	3.3	4.7	4.7	4.7	4.7	4.7
Hydropower	7	Avène	43.77	3.08	5	1960	1.9	60	33	%%	1	8	%%	6	8	%%	2.5	3.3	%%	3.3	3.3
Hydropower	8	Roselend	45.68	6.62	4	1962	3.2	149	185	%%	2	26	1	12	38	%%	2.9	3.9	2.9	3.1	3.9
Hydropower	9	Esparron	43.74	5.97	5	1967	3.8	55	80	%%	1	17	1	4	17	%%	2.5	4	2.5	4	4
Hydropower	10	Salagou	43.65	3.35	6	1969	7.5	45	102	%%	3	12	1	4	8	%%	3.3	3.3	3.3	3.3	3.3
Hydropower	11	Montbel	42.97	1.95	5	1982	5.5	45	60	%%	3	29	1	14	28	%%	2.7	3.2	2.6	3.2	3.2
Water-supply	12	Madine	48.92	5.73	5	1965	11	14	35	%%	%%	3	%%	1	3	%%	%%	2.8	%%	2.6	2.8
Hydropower	13	Laouzas	43.65	2.77	4	1965	4	40	45	%%	%%	2	%%	2	3	%%	%%	2.9	%%	2.9	2.9
Hydropower	14	Saint-Cassien	43.57	6.8	6	1966	3.7	40	60	%%	%%	19	%%	%%	9	%%	%%	4.2	%%	%%	2.9
Hydropower	15	Mont Cenis	45.2	6.95	4	1968	6.68	95	320	%%	%%	20	%%	8	31	%%	%%	3.4	%%	3.4	3.4
Hydropower	16	Der-Chantecoq	48.56	4.72	6	1974	48	14	350	%%	%%	1	%%	%%	%%	%%	%%	2.7	%%	%%	%%
Water-supply	17	Eaux Bleues	45.48	4.95	4	1975	3.5	10	24.5	%%	%%	5	%%	3	10	%%	%%	2.9	%%	2.9	3.9
Water-supply	18	Vesoul - Vaivre	47.63	6.12	2	1976	1	2	1.7	%%	%%	2	%%	4	36	%%	%%	2.9	%%	3.2	4.1
Water-supply	19	Villeneuve-de-la-Raho	42.63	2.92	2	1977	14	14	18	%%	%%	1	%%	2	27	%%	%%	3.4	%%	3.4	4.7
Hydropower	20	Naussac	44.72	3.83	7	1983	10.5	50	190	%%	%%	5	%%	%%	2	%%	%%	3	%%	%%	2.5
Hydropower	21	Grand Maison	45.2	6.12	5	1988	2.2	90	137	%%	%%	27	%%	6	27	%%	%%	3.7	%%	2.9	3.7
Hydropower	22	Pierre-Percée	48.47	6.92	3	1993	3.04	78	61	%%	%%	22	%%	22	28	%%	%%	4.9	%%	4.9	4.9
Water-supply	23	Orient	48.27	4.33	6	1966	23	18	205	%%	%%	%%	%%	%%	%%	%%	%%	%%	%%	%%	%%
Water-supply	24	Maine	47.45	-0.58	1.5	1970	1.5	4	6	%%	%%	%%	%%	4	16	%%	%%	%%	%%	3.1	3.3
Hydropower	25	Villerest	45.98	4.03	2	1984	7.7	59	127	%%	%%	%%	%%	%%	4	%%	%%	%%	%%	%%	2.9
Water-supply	26	Amance	48.34	4.51	3.5	1989	4.8	12	170	%%	%%	%%	%%	%%	%%	%%	%%	%%	%%	%%	%%

b)

N	Name	Mmaxdelay_1L[year]	Mmaxdelay_3L[year]	Mmaxdelay_10L[year]	Mmaxdelay_10km[year]	Mmaxdelay_30km[year]	Mmaxdelay_50km[year]	M1delay_1L[year]	M1delay_3L[year]	M1delay_10L[year]	M1delay_10km[year]	M1delay_30km[year]	M1delay_50km[year]	M_1[1L]	M_1[3L]	M_1[10L]	M_1[10km]	M_1[30km]	M_1[50km]
1	Grandval	7.24	15.29	3.31	4.59	7.24	7.24	4.59	4.59	3.28	4.59	4.59	4.59	2.7	2.7	3.3	2.7	2.7	2.7
2	Serre-Ponçon	6.64	13.10	1.31	5.64	19.20	13.10	5.16	2.48	1.28	5.64	3.16	2.48	2.5	2.6	3.4	2.7	3.1	2.6
3	Monteynard-Avignonet	1.31	1.31	0.31	1.31	0.31	0.31	0.28	0.28	0.28	0.28	0.28	0.28	3.4	3.4	3.4	3.4	3.4	3.4
4	Vouglans	2.47	2.47	2.47	2.47	2.47	2.47	2.47	2.27	0.29	2.47	2.47	2.47	4.6	3.1	2.6	4.6	4.6	4.6
5	Sainte-Croix	15.85	9.47	16.11	%%	9.46	9.46	15.85	3.55	0.13	%%	4.06	3.55	2.8	2.8	2.6	%%	2.7	2.8
6	Caramany	1.13	1.13	1.13	1.13	1.13	1.13	1.13	1.13	0.02	1.13	0.02	0.02	2.5	4.7	2.6	4.7	2.6	2.6
7	Avène	%%	7.18	18.66	%%	18.66	18.66	%%	7.18	3.85	%%	3.85	3.85	%%	2.5	2.9	%%	2.9	2.9
8	Roselend	%%	12.44	18.92	12.44	4.05	18.92	%%	6.80	0.31	12.44	2.81	0.31	%%	2.6	2.6	2.9	2.6	2.6
9	Esparron	%%	3.75	17.46	3.75	17.46	17.46	%%	3.75	0.07	3.75	0.07	0.07	%%	2.5	2.7	2.5	2.7	2.7
10	Salagou	%%	9.66	9.66	9.66	9.66	9.66	%%	1.27	1.27	9.66	1.27	1.27	%%	2.8	2.8	3.3	2.8	2.8
11	Montbel	%%	12.45	15.43	6.64	15.43	15.43	%%	6.64	3.89	6.64	4.15	3.89	%%	2.6	2.5	2.6	2.7	2.5
12	Madine	%%	%%	12.33	%%	7.74	12.33	%%	%%	7.19	%%	7.74	7.19	%%	%%	2.6	%%	2.6	2.6
13	Laouzas	%%	%%	11.74	%%	11.74	11.74	%%	%%	2.18	%%	2.18	2.18	%%	%%	2.5	%%	2.5	2.5
14	Saint-Cassien	%%	%%	8.10	%%	%%	6.05	%%	%%	0.26	%%	%%	1.78	%%	%%	2.6	%%	%%	2.5
15	Mont Cenis	%%	%%	15.06	%%	15.06	15.06	%%	%%	0.52	%%	0.52	0.52	%%	%%	2.5	%%	2.5	2.5
16	Der-Chantecoq	%%	%%	3.04	%%	%%	%%	%%	%%	3.04	%%	%%	%%	%%	%%	2.7	%%	%%	%%
17	Eaux Bleues	%%	%%	18.14	%%	18.14	9.29	%%	%%	8.30	%%	8.30	8.30	%%	%%	2.6	%%	2.6	2.6
18	Vesoul - Vaivre	%%	%%	6.22	%%	1.02	8.99	%%	%%	6.22	%%	1.02	1.02	%%	%%	2.9	%%	3.2	3.2
19	Villeneuve-de-la-Raho	%%	%%	1.84	%%	1.84	19.13	%%	%%	1.84	%%	1.84	1.84	%%	%%	3.4	%%	3.4	3.4
20	Naussac	%%	%%	10.79	%%	%%	11.46	%%	%%	8.57	%%	%%	11.46	%%	%%	2.7	%%	%%	2.5
21	Grand Maison	%%	%%	11.03	%%	7.69	11.03	%%	%%	1.20	%%	1.20	1.20	%%	%%	2.5	%%	2.5	2.5
22	Pierre-Percée	%%	%%	10.14	%%	10.14	10.14	%%	%%	10.14	%%	10.14	5.23	%%	%%	4.9	%%	4.9	2.5
23	Orient	%%	%%	%%	%%	%%	%%	%%	%%	%%	%%	%%	%%	%%	%%	%%	%%	%%	%%
24	Maine	%%	%%	%%	%%	2.66	11.66	%%	%%	%%	%%	1.31	1.31	%%	%%	%%	%%	2.8	2.8
25	Villerest	%%	%%	%%	%%	%%	5.33	%%	%%	%%	%%	%%	5.33	%%	%%	%%	%%	%%	2.9
26	Amance	%%	%%	%%	%%	%%	%%	%%	%%	%%	%%	%%	%%	%%	%%	%%	%%	%%	%%

Table 1: a) Reservoir geometry and triggering patterns using (Lr) normalized distance to reservoir; CumN and M_{max} are number of triggered event, and observed M_{max} value in $1L_r$, $3L_r$, $10L_r$ and 10, 30, 50 km distance from the reservoir, respectively. Reservoirs are sorted first by L_r triggering distance, second by impoundment times.
b) Time delay between M_{max} and first event (M_1) relatively to impoundment time. Values for $1L_r$, $3L_r$, $10L_r$ and 10, 30, 50 km distance from reservoirs.

a)

Group	Median	Mad	Median (other Res.)	Mad (other Res.)	p-value	Significance
1L (6)	0.17	0.12	0.05	0.02	0.0005429	Highly significant
3L (11)	0.06	0.03	0.04	0.03	0.005418	Highly significant
10L (22)	0.05	0.02				
all (26)	0.05	0.02				

b)

Group	Median	Mad	Median (other Res.)	Mad (other Res.)	p-value	Significance
10 km (9)	0.09	0.06	0.04	0.02	0.0002162	Highly significant
30 km (20)	0.05	0.02	0.03	0.02	0.03112	significant
50 km (23)	0.05	0.02				
all (26)	0.05	0.02				

Table 2: Triggering distance and reservoir length, for Lr distance and km distance triggering. a) Trigger in L_r distances. "MAD" is the median absolute deviation. The p-value is the value for the WMW one-tailed test, with alternative hypothesis that the median length for "near" triggering reservoirs minus the median length for other reservoirs is greater than 0 ; b) same as a) for km distance

Threshold ($1L_r$)	success rate (%, +/all)	
Length > 8 km	80%	5/6
Volume > 400 $10^6 m^3$	50%	3/6
Depth > -	0%	0/6
Surface > -	0%	0/6
Threshold (10km)	success rate (%, +/all)	
Length > 18 km	33%	3/9
Volume > 400 10^6 m^3	11%	1/9
Depth > 100 m	33%	3/9
Surface > -	0%	0/6

Table 3: Reservoir dimension thresholds and success rate for extracting trigger reservoirs when imposing no false alarm for reservoir dimension threshold. Top rows: Trigger reservoir in $1L_r$ - distance; bottom rows: Trigger reservoir in 10 km distance.

	Reservoirs					
	SP	SC	V	G	M	C
V	1	2	4	6	13	21
D	8	7	4	10	3	12
S	2	3	5	7	14	24
L	3	4	1	2	7	13
M_{max} (1L)	2.7	2.8	4.6	2.9	4.6	3.3
M_{max} (3L)	4.2	4.2	4.6	4.2	4.6	4.7

Table (4) : Ranking of French reservoir dimensions for trigger reservoirs within $1L_r$ distance: (V) Volume, (D) Depth, (S) Surface and (L) Length; Reservoir names as SP: Serre-Poncon; SC, Sainte Croix; V, Vouglans; G, Grandval; M, Monteynard; C, Caramany). Numbers are the ranking for the $1L_r$ triggering reservoirs according to reservoir geometry parameters given in Table (1) for the 26 reservoirs.

	Tectonic seismicity [1]	Reservoir Triggered seismicity [°]
Trigger	Tectonic mainshock	Reservoir impoundment
Source scaling	$M_o = \mu SD \cong \mu L^3$ $M \cong Log(M_o)$	$M_o{}^*_{reservoir} = \mu SD = \mu V_r \cong \mu L_r{}^3$ $M^*_{reservoir} \cong Log(M_o{}^*_{reservoir})$
Stress change - Value - Type	 $\Delta\sigma = 0.1–10$ Mpa Stress drop	 $\Delta\sigma = 0.5–1.5$ Mpa Reservoir depth
Triggered EQ -Distance -Coulomb stress change -M_{max}	 1-3L (aftershocks) $\Delta\sigma = 0.01–0.1$ MPa $<M_{max}> = (M_{ms} - 1.2)$	 1-3 L_r (RTS) $\Delta\sigma = 0.01–0.1$ MPa [2, 3, 4] $<M_{max}> < (M^*_{reservoir} - \alpha)$

Table (5): Triggered earthquakes in Tectonic and Reservoir impoundment context: M_o, M, the seismic moment and moment magnitude, respectively; μ the rock matrix shear modulus, S the fault surface that slips, in average, of a D value. M_{max}, the magnitude of largest triggered earthquake, i.e. the largest observed aftershock for tectonic events and the largest locally observed RTS event, respectively. <M> is the average magnitude value. $M^*_{reservoir}$ is the reservoir equivalent moment magnitude, using (L_r) the reservoir length. V_r is the reservoir volume. References for the tectonic seismicity are from e.g. [1]Scholtz (2002). Reference for RTS phenomenology are from [°] this study except, [2]Bell and Nur, (1978), [3]Roeloffs, (1988) and [4]Deng et al., (2010). See text for details.

a)

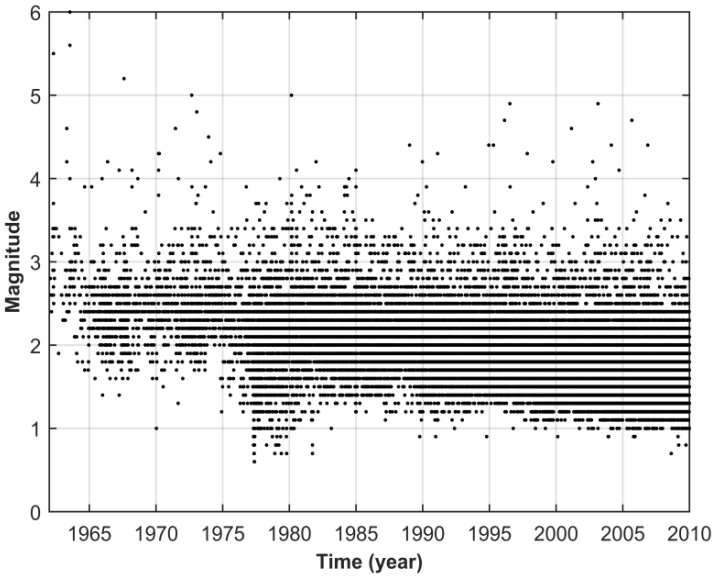

b)

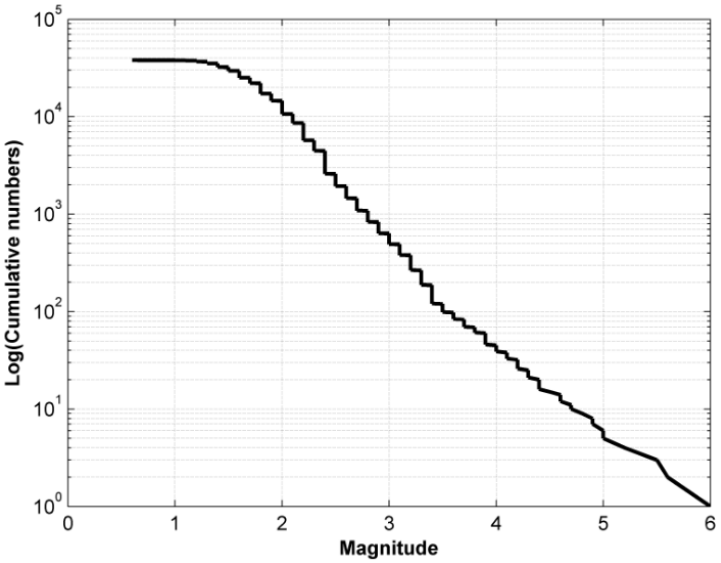

Figure 1: French Metropolitan Seismicity 1962-2009: a) Magnitude as a function of time. b) Frequency size distribution of all events (SI-Hex database, Cara et al. 2015).

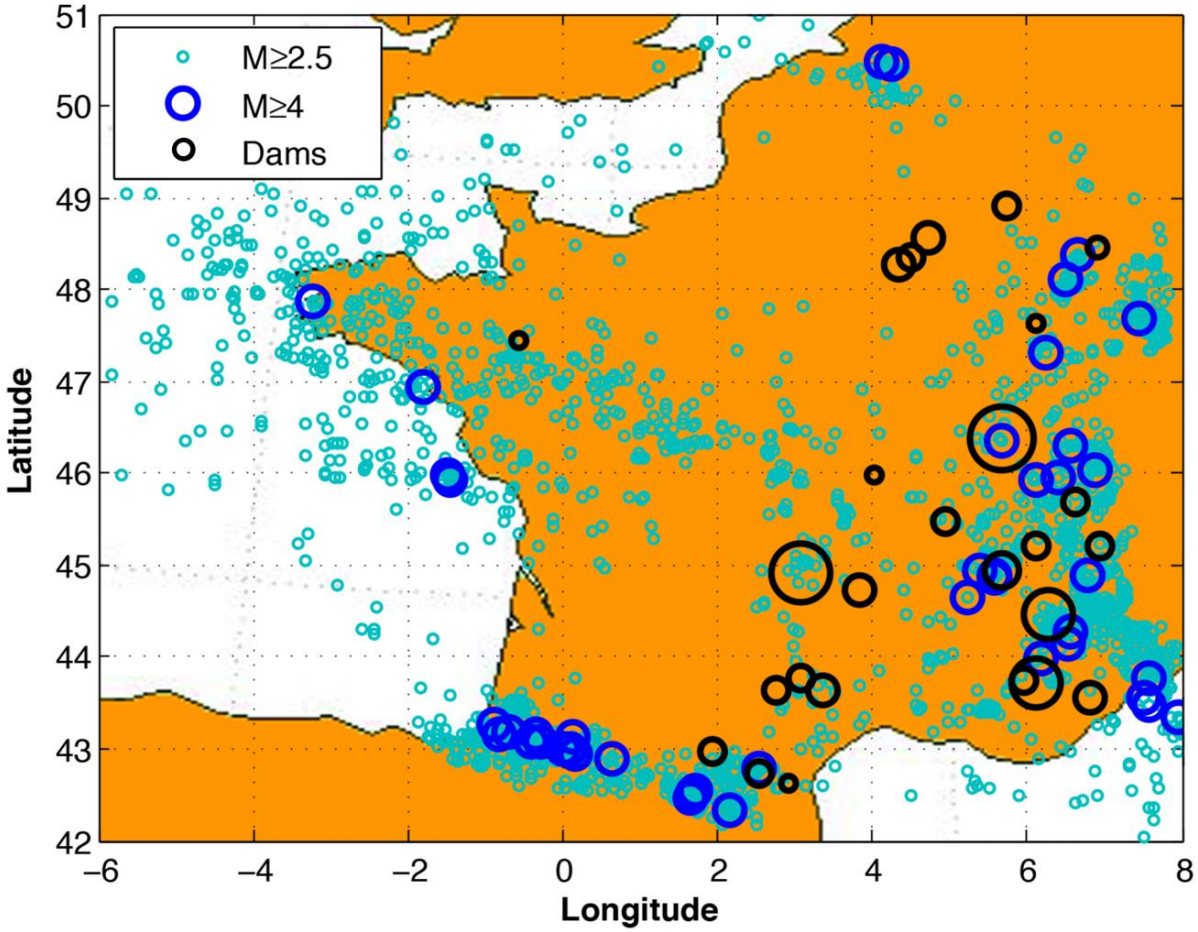

Figure 2: Seismicity map for metropolitan France, M2.5, 1962-2009 and the 26 reservoir locations we use in this study. Black circle sizes for reservoirs scale with reservoir lengths. Dark blue circles are M4 and above earthquakes. Small light cyan circles are M2.5-3.9 earthquakes. Catalogue from SI-Hex database, (Cara et al. 2015)

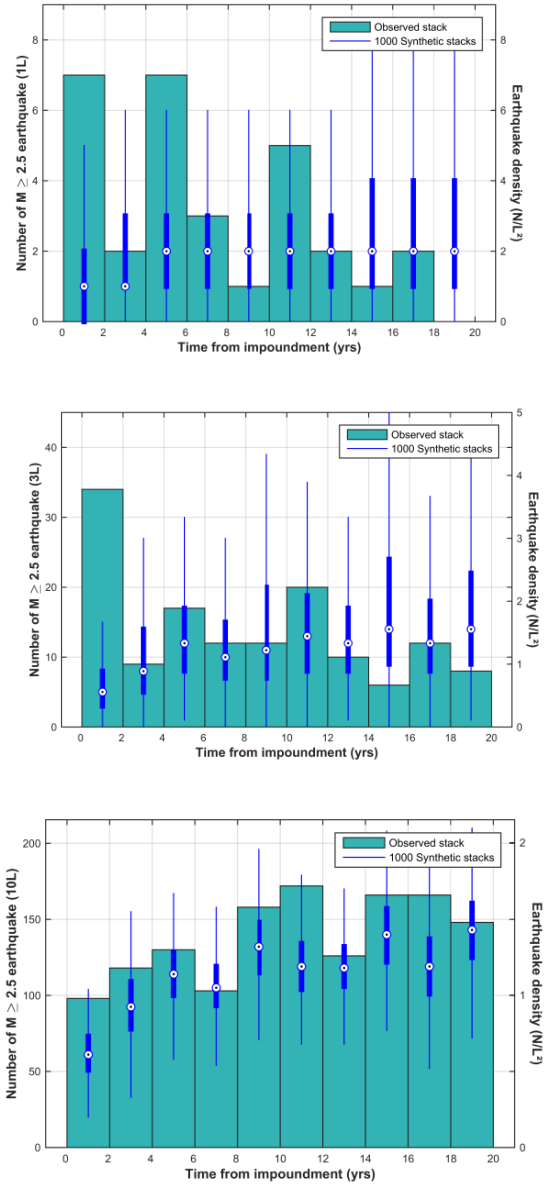

Figure 3: Average seismicity rate after impoundment time: data are stacked time series for earthquakes: top) $1L_r$, middle) $3L_r$, bottom) $10L_r$ distances from the reservoirs. Left vertical axis is the normalized seismicity rate density per surface units (N/L^2). Green boxes are observed seismicity rates. Light blue bars are 2 standard deviation values of the synthetic time series for 26 randomized reservoir locations (as averaged on 1000 series). Within 1-3 L_r distance from the reservoir, the observed stacked (green boxes) overpass the synthetic (blue bars) series in the 0-2 year time windows after impoundments.

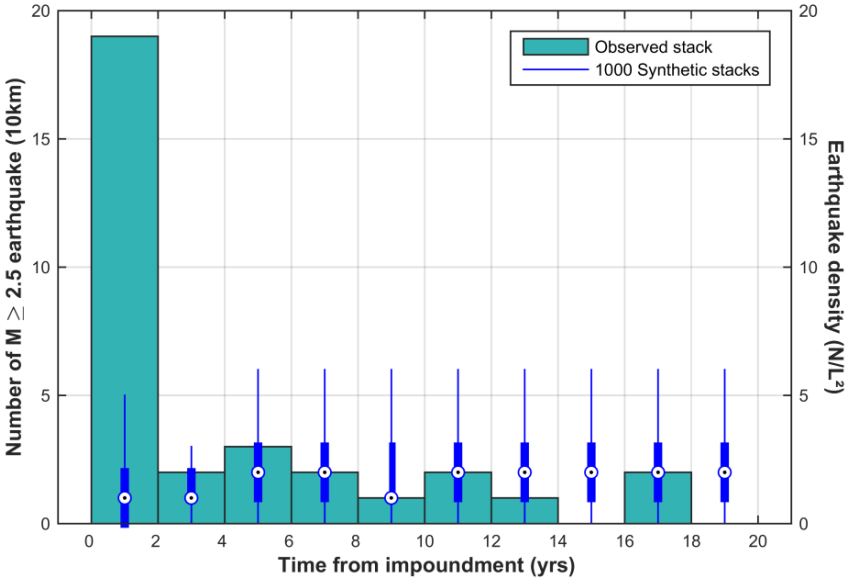
Observed stack
1000 Synthetic stacks
Number of M ≥ 2.5 earthquake (10km)
Earthquake density (N/L²)
Time from impoundment (yrs)
0
2
4
6
8
10
12
14
16
18
20
0
5
10
15
20

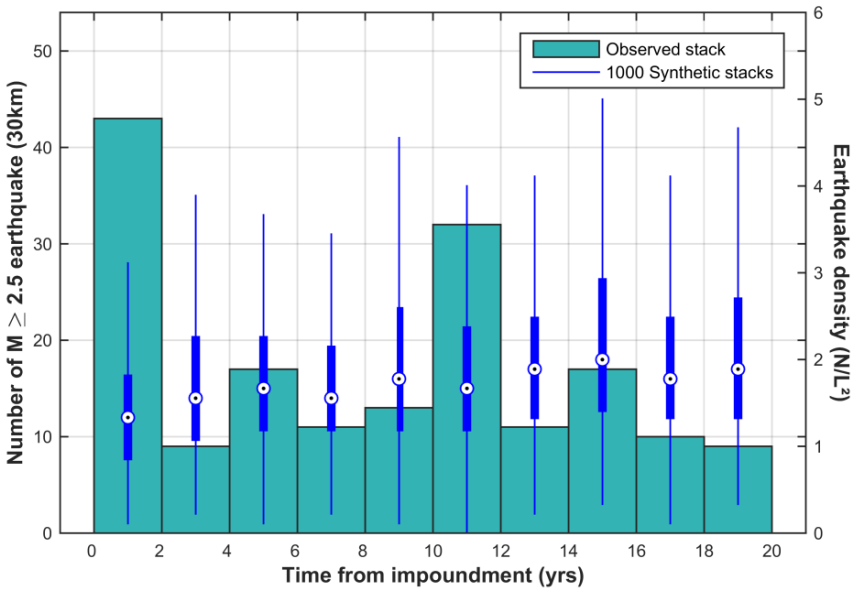
Observed stack
1000 Synthetic stacks
Number of M ≥ 2.5 earthquake (30km)
Earthquake density (N/L²)
Time from impoundment (yrs)
0
2
4
6
8
10
12
14
16
18
20
0
10
20
30
40
50
0
1
2
3
4
5
6

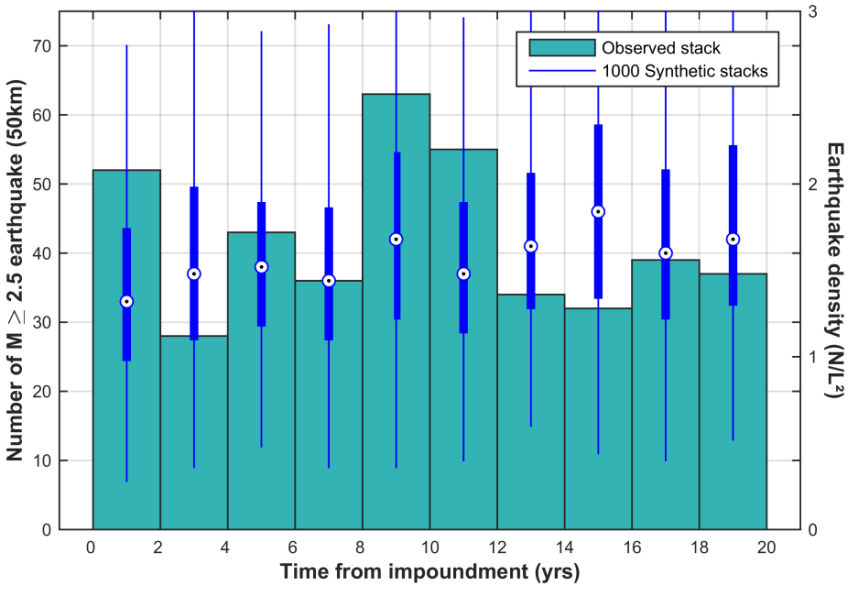

Figure 4: Same as figure (3) for 10-30-50 km distances.

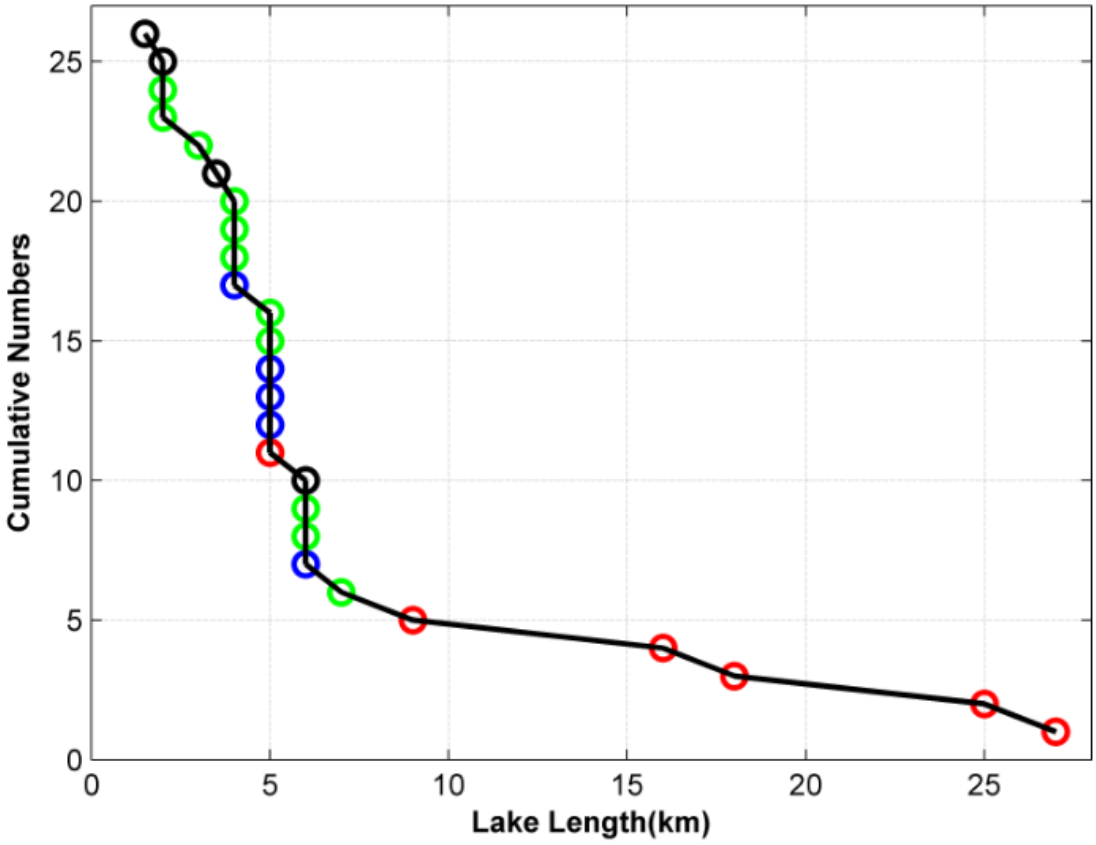

Figure 5: Cumulative distribution of reservoir lengths for the 26 reservoirs. Red, blue and green are reservoirs that trigger in 1, 3, 10 Lr-distance to reservoir, respectively.

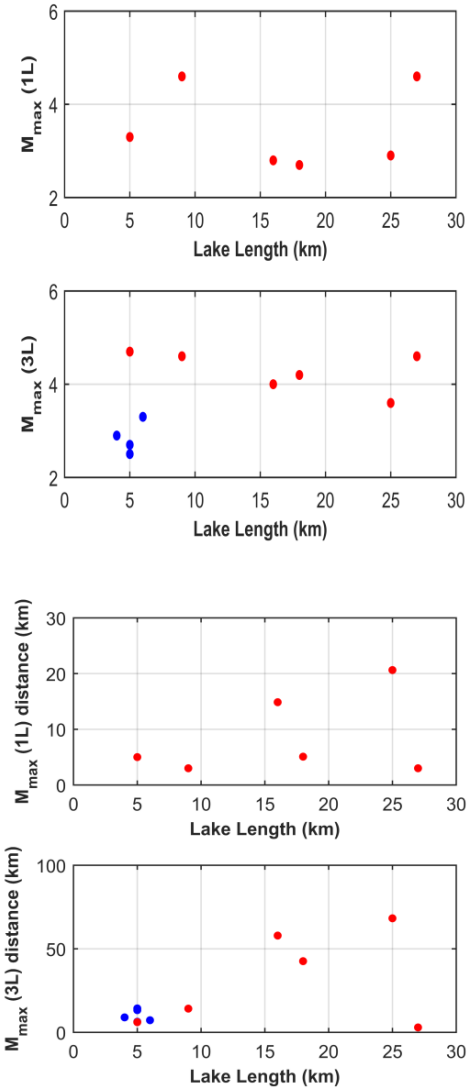

Figure 6: M_{max} values and distances to reservoir as a function of the reservoir lengths: (top) M_{max} value in $1L_r$-distance as a function of reservoir length; (bottom) M_{max} distance as a function of reservoir length; Red for reservoir triggering in $1L_r$, 10km; blue for triggering in $3L_r$, 30km distances. Note that when a color is still used for distance larger than the original definition (e.g. red in $3L_r$-distance) it corresponds to reservoir that triggers earthquake in $1L_r$ but also in $3L_r$ distances. This way, four over six of the reservoirs that trigger in $1L_r$ also trigger in $3L_r$ distances.

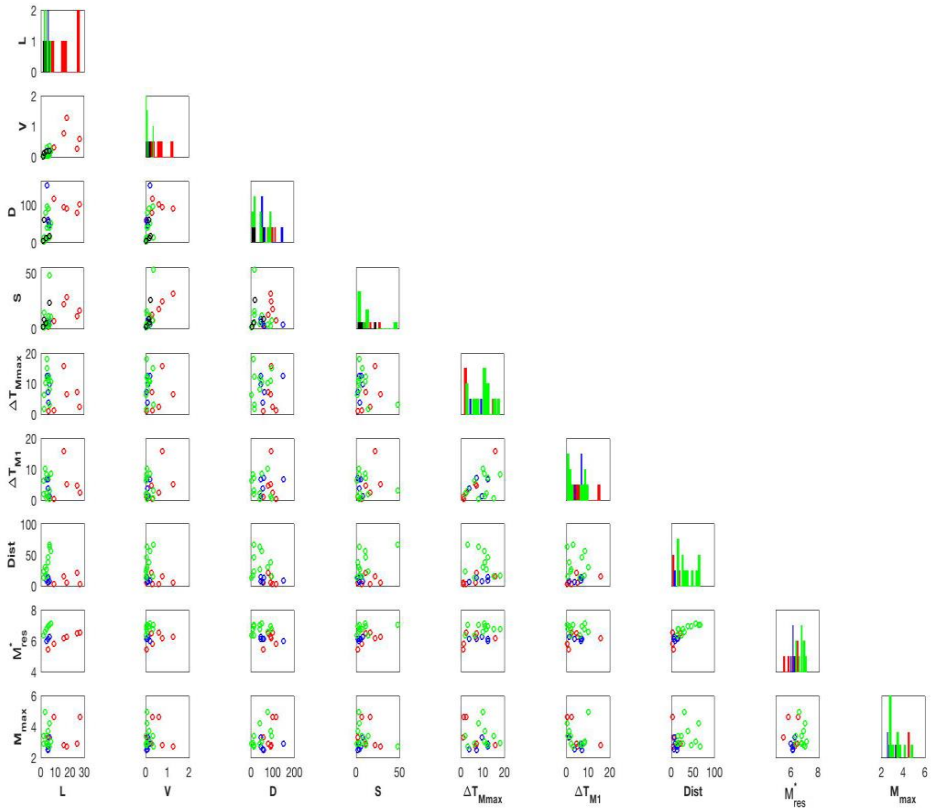

Figure 7: Features plot for L_r distances. Overall view of the distribution of the nine reservoir seismicity features (L, V, D, S, Dt_{max}, Dt_{M1}, Dist, M^*_{res} M_{max}) and their bivariate relations. Diagonal panels: normed histograms (color filled bins). Lower-diagonal panels: scatter plots. Notice that the x-axes are shared within columns. The diagonal panels are in units of density (not shown). Red, blue and green are for triggering in 1, 3, $10L_r$ respectively. Dt_{max}, Dt_{M1}, are time delays between M_{max}, and first event and the reservoir impoundment time. M^*_{res} is the proxy for the reservoir mainshock size as a $M^*_{reservoir}=M(L_r)$; L_r is the reservoir length (see text for details).

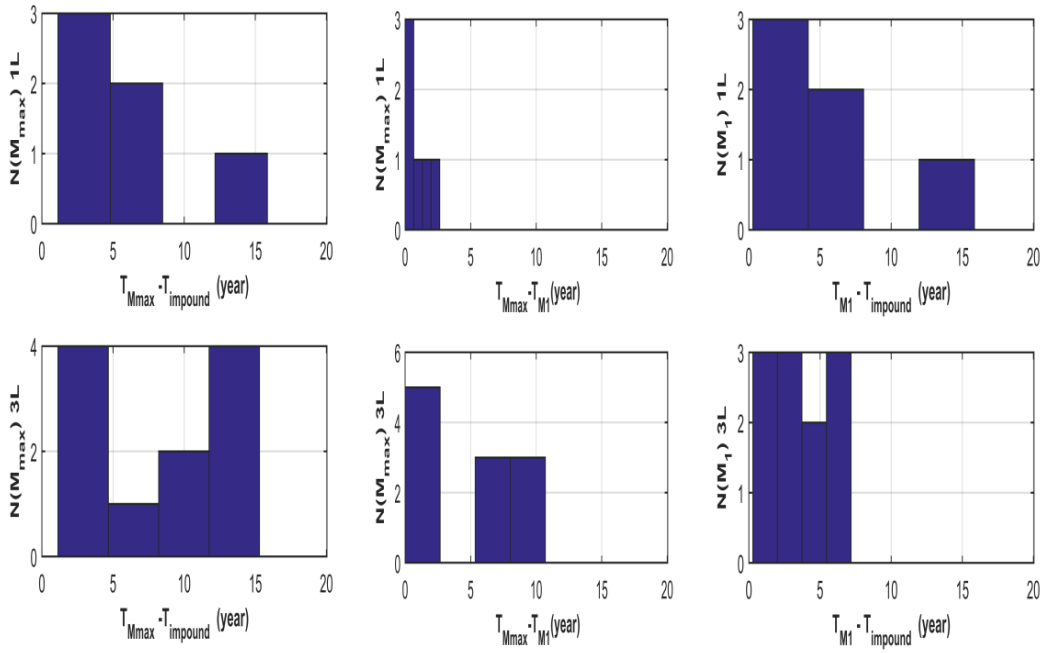

Figure 8: Distribution of time delays between M_{max}, M_1 (first event), and reservoir impoundment times. Column : Left) $M_{max}=f(t_{Mmax} - t_{impoud})$; middle) $M_{max}=f(t_{M1} - t_{impoud})$; right) $M_{max}=f(t_{Mmax} - t_{M1})$. Lines from left to right are M_{max} triggered in 1, 3 L_r-distance, respectively.

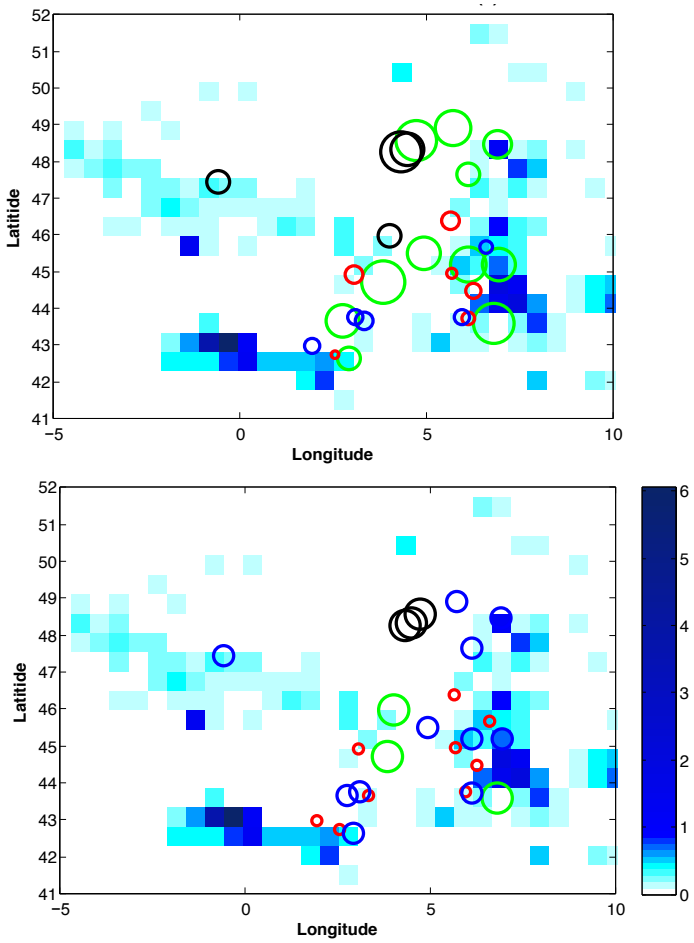

Figure 9: Tectonic seismicity rate and trigger reservoirs. (Top) L_r-distance to reservoir; (bottom) km-distance to reservoir. The circles are reservoir locations and the circle size scales with the reservoir triggering distance in either L_r (reservoir length) or km distances. The colors for circles are: red for triggering in $1L_r$, 10 km; blue for $3L_r$, 30 km; green for $10L_r$, 50 km. Black circles are reservoirs that do trigger neither in $10L_r$ nor in 50 km distances. The corresponding black circles are $10L_r$ and 50 km, respectively. The sizes of the others reservoir circles are $1L_r$, $3L_r$, $10L_r$ and 10, 30, 50 km for red, blue and green trigger reservoirs, respectively. Seismicity density is the key for square colors shading in yearly M2.5 event rate per 50x50 km^2 cell.

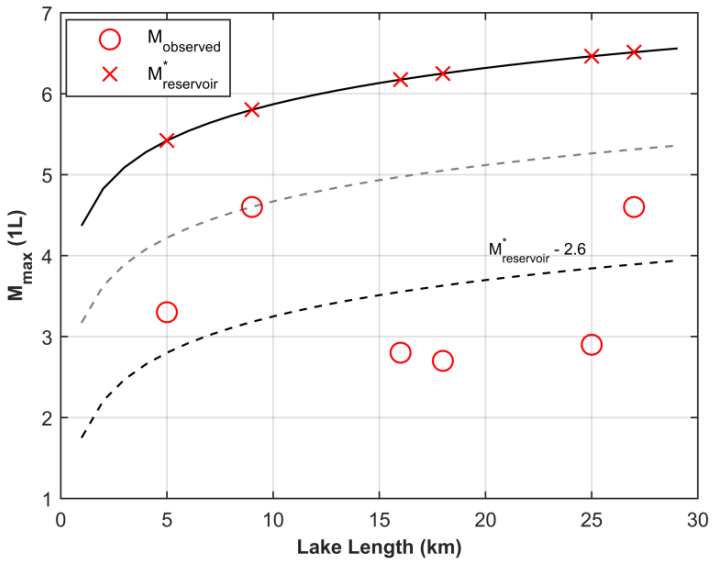
M observed
M* reservoir
M* reservoir - 2.6
M max (1L)
Lake Length (km)

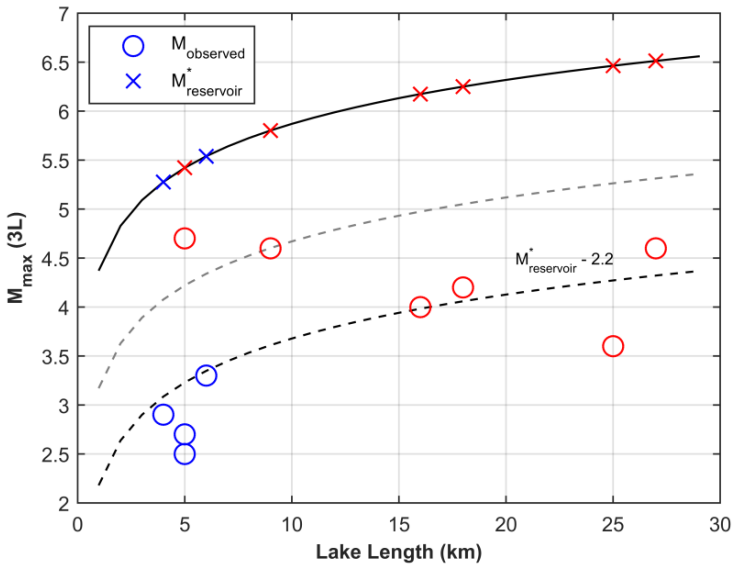
M observed
M* reservoir
M* reservoir - 2.2
M max (3L)
Lake Length (km)

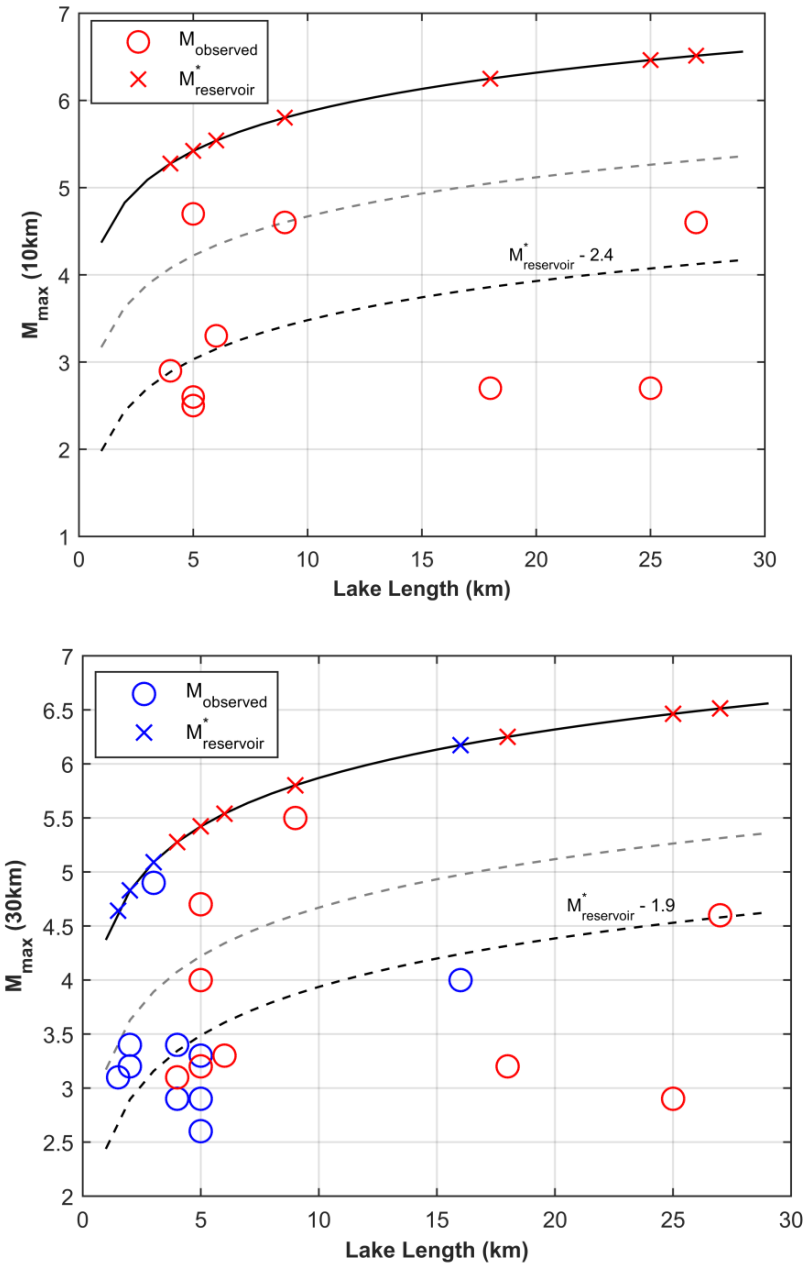

Figure 10: Observed M_{max} values and equivallent $M^*_{reservoir}$ as a function of reservoir length. M_{max} is the observed value within 1-3L_r (top) and 10-30 km (bottom) distance; $M^*_{reservoir}$= $M(L_r)$, L_r being reservoir length; $M(L_r)$ is from Wells and Coppersmith (1994). Red and blue dots are triggering in 1L_r, 10 km and 3L_r-30km distances. Curves are $<M_{theo}> = M^*_{reservoir} - \alpha$: from top to bottom, α=0, α=1.2 i.e. Bath law for tectonic aftershock. α values for the lowest curve are 2.6, 2.6, 2.4, 1.9 for 1-3Lr, 10-30 km distances respectively. See text for details

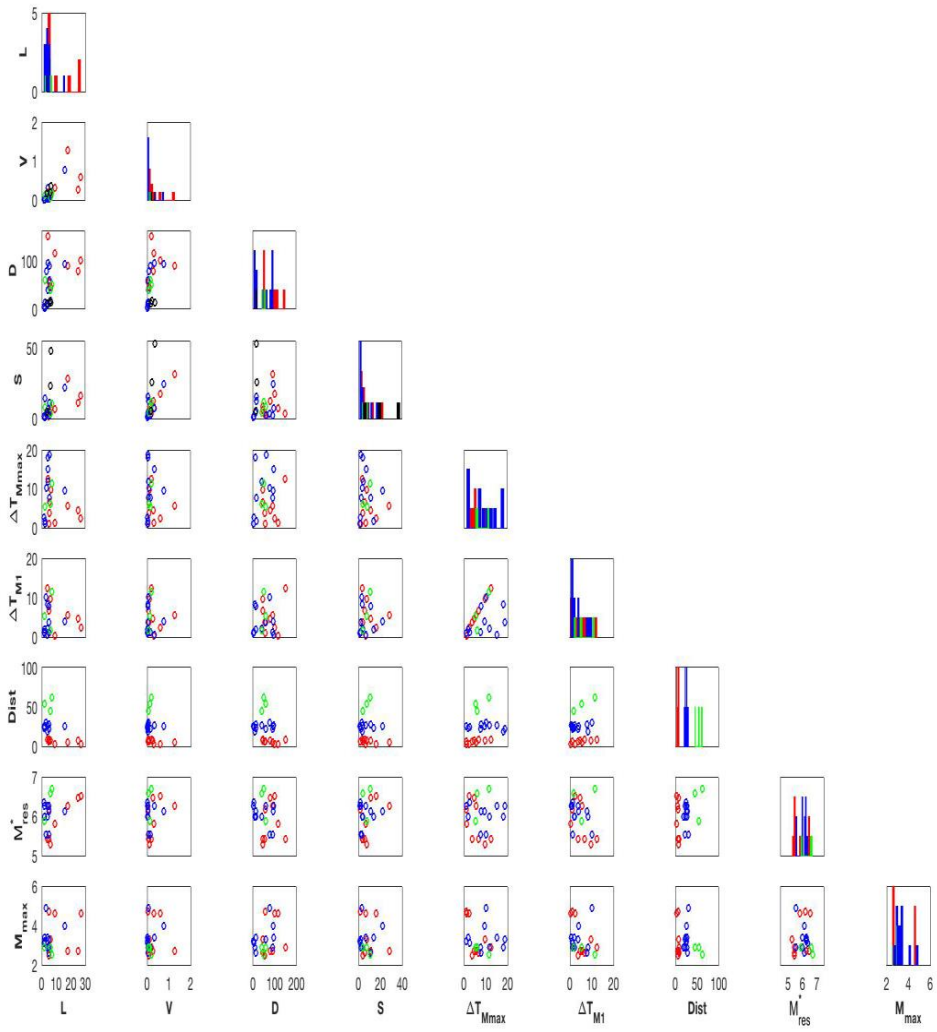
L
V
D
S
ΔTMmax
ΔTM1
Dist
M*res
Mmax

Figure A1: Feature plot for km distance: Same as Figure (7) for 10, 30, 50 km.

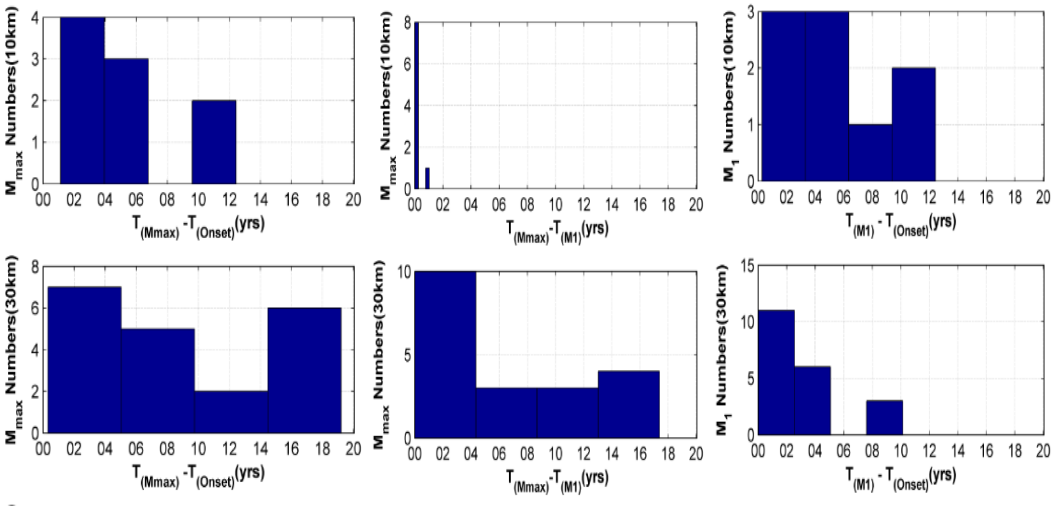

Figure A2: Same as Figure (8) for trigger in 10, 30, 50 km distance, respectively.